CHPATER 2

EPITAXY and MATERIAL CHARACTERIZATIONS OF GAN, ALGAN AND ALGAN/GAN THIN FILMS

2.1 Introduction to MOVPE System

GaN is one of the most promising materials for applications in high frequency power electronics as well as opto-electronics in the green to ultraviolet range of spectrum. It has many amazing properties, including high thermal conductivity, wide bandgap energy and high breakdown field and electron mobility. These general properties lend themselves to exploitation in nearly any electronic device with special applications in high powe, high frequency applications, and used in hostile conditions (such as high temperature probes). Commercial GaN based LEDs and lasers are currently available, more devices will become available in the future. Some of the most interesting devices are made from GaN when it is alloyed with aluminum or indium. Band discontinuities between GaN and: AlN ~ 2.0 eV conduction band, 0.7 eV valence band; InN ~ 1.0 eV conduction band, 0.43 eV valence band; and for cubic GaN and GaAs ~ 1.84 eV valence band. A.V. Figure 2-1 is the theoretical phase diagram demonstrated by Davydov *et. al.*, which was assessed by CALPHAD method [1]. As can be seen, in STP, gallium nitride is very unstable. Gallium nitride sublimates incongruently by decomposing into nitrogen-rich gas and gallium-rich liquid, but can melt congruently at high nitrogen pressure (≈4.9 GPa). That's also why GaN substrate is not available by conventional crystal growth method (CZ or FZ Method). For thermodynamics concern, it is true, but not for thermokinetics consideration.

In general, the GaN epitaxial layer is grown on sapphire substrate by using the MOVPE method, even though the reactive MBE [2-3] method have been adapted to grown high quality GaN film by using the N_2 gas as the group V source. The MOVPE technique was invented in 1968. Manasevit firstly demonstrated that using triethylgallium (TEGa) and arine (AsH_3) to deposit single crystal GaAs pyrolytically in an open tube cold-water reactors [4]. Soon after, Manasevit applied this technique to grow GaN onto sapphire substrates [5]. Since the GaN substrate is still not available for practical applications. Sapphire and SiC are the most often used. Organometallic group III sources are either liquid, such as trimethylgallium (TMGa), triethylgallium (TEGa), trimethylaluminum (TMAl) and triethylaluminum (TEAl), or solid such as trimethylindium (TMIn). For III-nitrides growth, group V source is usually ammonia (NH_3). Dopant materials can be metal organic precursors such as dimethylzinc (DMZn), cyclopenta dienyl magnesium (CP_2Mg) and hydrides of silane (SiH_4) or disilane (Si_2H_6). MOCVD growth of GaN involves the pyrolysis of a vapor phase mixture of NH3, most commonly, trimethylgallium (TMG) or triethylgallium (TEG). Free Ga atoms and ・NH_x radicals (x=1or 2) are formed and these species recombine on the hot substrated surface in an irreversible reaction to form GaN. The chemical reaction for GaN epitaxy in a MOVPE process could be tentatively written:

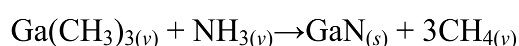

$$Ga(CH_3)_{3(v)} + NH_{3(v)} \rightarrow GaN_{(s)} + 3CH_{4(v)}$$

Gowth is carried out in a cold-wall stainless reactor in flowing H_2 at high temperatures. Figure 2-2 shows the schematic plot of the MOCVD reactor including the in-situ measurement system. Not only the thermodynamics is concerned, but also the kinetics of growth mechanisms at solid/vapor interface in the MOCVD should be

very carefully considered. For GaN, especially, the lacking of proper lattice-matched substrate makes it difficult to grow high quality thin films. Sapphire is the most used substrate for GaN thin film growth. Due to the large lattice mismatch, a low-temperature buffer layer is always needed to serve as a nucleation layer. A GaN film was then deposited on the nucleation layer. As the film grows, the crystals originated from each nucleus coalesce due to the dislocation annihilation and finally become a single crystal film.

A spectral reflectivity measurement system was used to monitor the thickness and optical constants of transparent GaN epitaxial layers on transparent sapphire substrate [6]. This is a real-time monitoring system, very similar to reflection high-energy electron diffraction (RHEED), which has been widely used for the study of crystal growth in MBE or MOVPE. However, the probe used here is narrow bandwidth light stylus instead of the electron beam. As shown in Fig. 2-2, a tungsten-halogen bulb was used as light source ranged from approximately 380 nm to 3000nm. The light is delivered through a fiber optic cable assembly and reaches the surface of the sample as a light stylus. The reflectivity is recorded with time. The basic theory behind the expected sinusoidal reflectance oscillations is briefly summarized below from Pedrotti and Pedrotti [7]. Referring to Fig. 2-3, it follows from thin-film interference or Fabry-Pérot interference theory. Provided the film material is a transparent dielectric material (without considering the absorption by the film, and surface roughness scattering), the reflectivity will be proportional to the cosine of the phase difference, $\Delta\varphi$, between the reflections from the air-film interface and the reflections from the underlying film-substrate interface. The phase difference can be translated into a path length difference via the equation:

$$\Delta path = 2 n_2 Z \cos\beta$$

Thus the change in reflectivity as a function of time, $\Delta R(t)$, can be expressed as a function of film thickness, index of refraction, and free-space wavelength of the incident light:

$$\Delta R(t) = R_0 \cos(\Delta\phi(t)) = R_0\left(\frac{4\pi n_2 Z(t)}{\lambda_0}\right)$$

Assume the rate of change of the thickness, or growth rate, *G*, is constant. The above equation is now:

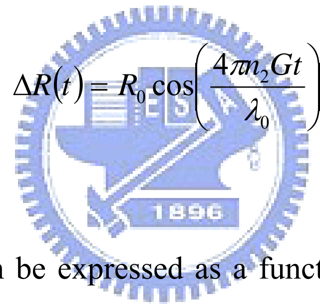

$$\Delta R(t) = R_0 \cos\left(\frac{4\pi n_2 G t}{\lambda_0}\right)$$

The oscillation frequency can be expressed as a function of index, growth rate, and free-space wavelength of the incident light:

$$f_{osc} = \frac{2 n_2 G}{\lambda_0}$$

By fitting the growth oscillation frequency, as well as assuming a known wavelength and index of refraction, the growth rate of the film can be easily computed.

In the following sections, for device requirements, some fundamental studies for GaN and AlGaN epitaxy are performed. Since each single layer is the foundation for device applications. All the single layers were characterized by PL, XRC, Hall measurement and relative materials analysis if necessary in order to realize epitaxy

optimization. Most of importance is the PL study involving the near-band-edge emission of GaN and the 2DEG phenomena at low temperatures.

2.2 Growth and Characterizations of undoped GaN and AlGaN Epilayers

An AlGaN/GaN heterostructure is essential in a nitride-based heterostructure field effect transistor. High-quality crystal is needed in fabricating a high performance device. However, due to the lack of a suitable substrate with structure and thermal matching to GaN, it is quite difficult to grow a high-quality GaN film. For years, the concept of mosaic nucleation layer has been used to overcome the large mismatch in the lattice difference between the substrate and epitaxial film. I. Akasaki, *et al.* were utilized the low-temperature AlN as a buffer layer prior to the epitaxial film [8]. Nakamura *et al*. had used low-temperature GaN instead of AlN as buffer layer also obtained the excellent crystal quality [9]. Kuznia *et al.* compared the qualities of the top GaN films on the GaN and AlN buffer layers and found that GaN films using an AlN as the buffer layer [10] seemed to have higher mobility and lower carrier concentration, though the effects of the GaN buffer layer were not very different from those of the AlN buffer layer.

To modify the growth procedure, several ways had been found to improve the film quality of the GaN layers. First, before the growth of the GaN epitaxial film, the sapphire substrate baked at 1100 ºC for 10 minutes in the H_2 atmosphere in order to clean the contaminated surface. Second, before the GaN layer being deposited, the low-temperature grown AlN layer was used as the buffer layer to improve the film quality. Akasaki *et al*. had attained obvious improvements of the the GaN epitaxial film by using AlN buffer layer. Nakamura also achieved the same results by using the

GaN buffer layer. Because the lattice mismatch of GaN on sapphire is less than that of AlN on sapphire, the comparison of the film quality for the GaN epitaxial film grown on AlN or GaN buffer layer is difficult. Therefore in this study, we take advantage of the GaN buffer layer and homoepitaxial growth to obtain high quality GaN films. The sapphire was baked at a high temperature in a NH_3 atmosphere before the growth of the low temperature GaN buffer. The effects of different pre-treatments and buffer layers on the GaN film quality are studied. In addition, the growth mode of the GaN film proposed by Akasaki *et al*. is also modified in this study.

2.2.1 GaN films grown on sapphire substrate

It is difficult to obtain a lattice-matched substrate for GaN; *c*-face (0001) sapphire has been successfully used as the substrate to grow GaN film by MOCVD growth method. Because of the large differences in lattice constant and thermal expansion coefficient between the sapphire substrate and GaN film, the performance of the GaN-based devices depends critically on the initial grown layer which determines the growth of the misfit dislocations and polarity related defects. Therefore, a low-temperature-grown buffer layer is required for growing good quality GaN epitaxial layer. The quality of the GaN epitaxial layer is sensitive to the growth method of the buffer layer. The low-temperature-grown GaN (LT-GaN) buffer layer could be amorphous. The crystal structure of the GaN buffer layer was transformed from an amorphous structure to a crystalline structure since it went through the annealing procedure from 525 ℃ to 1025 ℃ before the GaN layer growth. Thus, it is interesting to study the correlation of the buffer layer thermal treatment process of the buffer layer and the electrical characteristics of the GaN epitaxial layer growth. In this study, we report the effect of thermal annealing on the properties of the GaN

epitaxial layer growth. *In situ* thermal treatments with different ramping rates are conducted between the growth of the buffer and the epitaxial layers. The electrical properties of the GaN epitaxial layer were measured by Hall measurement. The crystallinity was studied by double-crystal x-ray rocking curve diffraction (DC-XRD).

The GaN films were grown by LP-MOCVD on polished optical-grade *c*-face (0001) sapphire substrates. Optical grade polished (0001) orientation (*c*-face) sapphires were used as the standard substrates for the GaN epitaxial growth. The sapphire substrates were heated at 1100 ºC for 10 minutes in H_2 and 10 minutes in the mixture of H_2 and NH_3 before the growth. This step was meant to clean the contaminated surface. Then, the substrate temperature is lowered to 525 ºC to grow the GaN buffer layer. The flow rates of H_2, and NH_3, and TEGa were 1000 sccm, 1500 sccm, and 8.3 μmole/min, respectively. The substrate temperature was then raised to 1000 ºC to grow the GaN epitaxial layer.

During the period of GaN growth at 525 ºC, the thicknesses of the GaN buffer layer was varied to decide the optimum thickness of the LT-GaN buffer layer by observing the optical and electrical properties. The total film thickness was controlled at about 1 μm and the thickness of the LT-GaN buffer layer varied from 20 nm to 75 nm. The thickness of the LT-GaN buffer layer was examined by the measurement of the thickness of the LT-GaN buffer layer grown for 15 minutes by using cross-session scanning electron microscopy (SEM). The crystalline structure of the GaN epitaxial film on the LT-GaN buffer layer is investigated by the SEM and the X-ray diffractometer. SEM was used to observe the surface morphology and film thickness and the X-ray diffractometer was used to check the crystal quality. The Hall-effect measurement was performed by the *van der Pauw* method at room temperature and liquid nitrogen temperature. The indium drop was annealed in forming gas (N_2: H_2 = 10:1) at 550 ºC for 10 minutes to form Ohmic contact for Hall measurement.

Sapphire was placed on a graphite susceptor in a horizontal type reactor with a RF heater. Triethylgallium (TEGa) and ammonia (NH_3) were used as the Ga and N sources, respectively. The carrier gas was hydrogen (H_2) and the growth pressure was kept at 76 torr. Before growing GaN films, the sapphire substrates were treated by thermal baking at 1100℃, to remove the contamination on the sapphire. The GaN buffer layer was grown at 525 ℃, which is lower than the normal-growth temperature of 1025 ℃ for the GaN epitaxial layer. The thickness of the buffer layer is about 100Å. After growing the buffer layer, the temperature was raised to 1025 ℃ to grow the GaN epitaxial layer. In this study, six samples with the GaN buffer layer and different temperature ramping rates were prepared. The ramping time, $\mathbf{t_1}$, was varied from 5 min to 40 min which corresponding to temperature ramping rate from 12.5 ℃/min to 100 ℃/min. Figure 2-4 shows the temperature-time profile for the growth process. After the thremal treatment, the GaN epitaxial layer was grown at 1025 ℃ with a thickness of 1.3 μm. The samples were then measured by DC-XRD. The FWHM of the DC-XRD as a function of the ramping rate is shown in Fig. 2-5 and the data was used as an indicator for the film quality. We observe that the value of FWHM strongly depends on the thermal treatment. The smallest FWHM (330 arc second) occurred at a ramping rate of 20℃/min. The carrier concentration and the electron mobility were measured by the Hall Effect at 77 K and 300 K. Figure 2-6 shows the measured Hall mobility and carrier concentrations verse the ramping rate at 300K. It clearly shows that the ramping rate has strong influences on the carrier concentrations of the GaN films. The lowest carrier concentration measured at room temperature was 1.7×10^{17} cm^{-3} , which also occurs at a ramping rate of 20 ℃/min. The room temperature mobility was 90 cm^2/Vs and 435 $cm^2/V{\cdot}s$ at ramping rate of

100 ℃/min and 20 ℃/min respectively. From Fig. 2-5 and Fig. 2-6, we found that the GaN film has the best electrical properties at a ramping rate of 20℃/min.

When the ramping rate is higher than 20 ℃/min, i.e, when the annealing of the buffer layer is 25min long, the mobility decreases with the increase in the ramping rate as indicated in Fig.2-6. This observation may be due to the large thermal expansion coefficient difference between GaN films and the sapphire substrate. The thermal expansion coefficients for sapphire were $\Delta a/a=7.5\times 10^{-6}$/K and $\Delta c/c=8.5\times 10^{-6}$/K from Landolt-Borntein [11]. The thermal expansion coefficients of GaN measured by Maruska *et. al.* [12] were $\Delta a/a=5.59\times 10^{-6}$/K and $\Delta c/c=3.17\times 10^{-6}$/K at 300 K. Since the thermal stress is proportional to the difference of the thermal expansion coefficient and the temperature gradient between GaN and sapphire, at the higher ramping rate condition, there was not enough time for the thermal stress to relieve and the crystal quality of the GaN buffer layer degraded and result in an inferior GaN epitaxial layer. It was also believed that the ramping process performed as an annealing process. The LT-GaN starts the crystal coalescence mechanism and created small nucleation sites during temperature raping. As the ramping rate was large, there was not enough time to obtain oriented nucleation sites. Wickenden *et. a l.* [13] suggested that the low-temperature-grown buffer layer has a measurable crystalline component with very small crystal size, upon annealing at high temperature, the crystal size increases and the crystal quality improves significantly. Because the higher ramping rate has a shorter annealing time, the crystals of the GaN LT-GaN layer did not have enough time to coarsen, and thus the quality of the GaN film grown is poor. On the other hand, when the ramping rate is lower than 20 ℃/min. The mobility decreases with the decrease of ramping rate. This is due to a longer annealing time could induce the dramatic re-evaporation of GaN buffer layer. One of

the possible reasons is that the thickness of the buffer layer annealed by a low ramping rate would be thinner than that by a higher ramping rate. The effects of buffer layer thicknesses on the quality of the following grown film have been described by Kuznia *et al*. [14]. It indicates that the thickness of the buffer layer has a critical thickness, smaller or larger than the critical thickness will have inferior film quality. Therefore, a thinner GaN buffer layer for the low ramping rate will degrade the quality of the following grown GaN epitaxial layer. Another possible reason is that the re-evaporation effect due to the low ramping rate caused the decomposition of GaN into Ga metal and nigrogen which resulted in the change in the crystalline sizes of the nucleation layer and consequently affect the crystal quality of the GaN epitaxical layer grown.

The maximum electron mobility also occurred at the ramping rate of 20 ℃/min. This result indicates that the thermal annealing process does reduce the impurity concentration of the GaN epitaxial layer. The FWHM of the photoluminescence band-edge peak of GaN epitaxial layer at 10K versus temperature ramping rate is shown in Figure 2-7. The lowest value of the FWHM is about 12 meV at 20℃/min ramping rate. The broaden PL FWHM of the sample with high and low temperature ramping rates may be explained as follows: (1).There are more defect-related states existing in the film. (2).The nucleated sites are not along the (0001) axis with high temperature ramping rate. (3).The re-vaporization process at low ramping rate reduces the number of LT-GaN nucleated sites. The direction and number of LT-GaN nucleation sites have strong influence on the GaN film growth process [15].

In conclusion, we have studied the effect of the thermal annealed GaN buffer layer on the quality of the GaN epitaxial layer. Different temperature ramping rates were studied and the optimum annealing conditions. The electron mobility, the carrier concentration, the x-ray, and PL data of the GaN epitaxial layer obviously indicate the

film quality is strongly dependent on the ramping rate of the annealing process. The ramping rate of 20 ℃/min has been found to be the optimum ramping rate and the GaN epitaxial layer grown has a high electron mobility of 435 $cm^2/V \cdot s$ and a low intrinsic carrier concentration of 1.7×10^{17} cm^{-3}. Two different processes may have strong influences on the electronic property of the GaN film. One is the poor oriented nucleation sites at the high ramping rate and another is re-evaporation process of the GaN at the low ramping rate.

2.2.2 AlGaN films grown on sapphire substrate

During the growth, the sapphire substrates were placed on a graphite susceptor in the MOCVD reactor. Triethylgallium (TEGa), trimethylaluminum (TMAl) and ammonia (NH_3) were used as the Ga, Al and N sources. And the diluted SiH_4 gas mixed with H_2 gas was used as the n-type dopant during the growth of the AlGaN films. The V/III ratio, i.e. N/(Ga+Al) mole ratio, was kept at about 4000 in this growth system and the group III metalorganic sources were consisted of Ga and Al. The carrier gas is hydrogen (H_2) and the growth pressure was kept at 200 mbar. Before growing GaN films, the sapphire substrates were treated by thermal baking at 1190°C to minimize the surface contamination. The optimum LT-GaN nucleation layer with a 0.5μm-thick GaN top buffer layer were used to grow AlGaN epitaxial layers with better quality on the sapphire substrates.The LT-GaN buffer layer was thermally treated at 1130 °C for 5 min, and the top GaN buffer layer was deposited at 1130 °C. After the growth of the GaN film, the growth temperature and chamber pressure was switched to 1160 °C and 50 mbar to grow the AlGaN layers.

DC-XRD (double-crystal x-ray rocking curve diffraction) measurements were tested to analyze the crystalline properties, the x-ray diffraction curve of GaN (0004),

$Al_xGa_{1-x}N$ (0004) peaks were shown in Fig. 2-8. The thickness and the surface morphology of AlGaN/GaN double layers were observed from the SEM photograph in Fig. 2-8. The electrical properties of AlGaN epitaxial layers on GaN second buffer layers are also measured by Hall Effect measurement. Photoluminescence (PL), and cathodoluminescence (CL) were also used to evaluated the luminescence properties. The Al content of AlGaN layer was 0.095 as determined from the splitting angle between GaN and AlGaN peaks in x-ray diffraction curves. The electron mobility and carrier concentration were about 635 $cm^2/V{\cdot}s$ and 1.4×10^{17} cm^{-3} for the AlGaN epitaxial layer grown at 300K. The AlGaN peak, GaN peak and yellow peak were observed from PL and CL spectra at RT as shown in Fig. 2-9. Both of the AlGaN peak s were located at 350nm in PL and CL spectrums, and the Al content of AlGaN films was 0.09, the result is similar to that from the x-ray diffraction curves.

The relationship of the Al/(Al+Ga) mole fraction in the gas phase and the solid film composition was also studied. The V/III ratio was fixed at 10000 during these series of AlGaN/GaN epitaxial grwoth in the MOCVD system. The Al/(Al+Ga) mole flow ratio as the function of the TMAl flow rate is shown in Fig. 2-10. The Al content in AlGaN layers calculated from the Vegard's law as the function of the TMAl flow rate also shown in Fig. 2-10.

Vegard's law.

$$\left[\frac{\Delta c}{c}\right]_{\perp} = \frac{\sin\theta_B}{\sin(\theta_B + \Delta\theta)} - 1$$

$$c_{AlGaN} = c_{GaN} + \Delta c = x \cdot c_{GaN} + (1-x)\cdot c_{AlN}$$

The Al/(Al+Ga) mole flow ratio shows the same values as the Al content calculated from the Vegard's law. The Al content was proportional to the Al/(Al+Ga) mole flow ratio in the gas phase but did not show linear dependent to the TMAl source flow rate.

2.3 Near-Band-Edge Emissions of GaN at Low Temperatures

It is of crucial importance to establish the value of the fundamental excitonic transition in unstrained GaN. Skromme [16] measured the radii of curvature of the GaN epilayers grown on *c*-Al_2O_3 and *c*-6H-SiC substrates. He found that the value of the excitionic bandgap in unstrained GaN is 3468±2 meV at 2 K. Figure 2-11 is the sketch of the construction of the exciton states from the combination of conduction and valence band Bloch states [17-21]. Many researchers have been exciting samples grown along the [0001] direction on *c*-plane oriented substrates. This makes it easy to detect Γ_5 dipole excitons allowed in σ polarization. Hoffman and Eckey [22] decided to measure the energy of the Γ_6 mode forbidden dipole at the zone centre. They used the objective of a microscope to excite and collect the free exciton photoluminescence (PL) emitted along the [10-10] direction from a thick sample grown by hydride vapour phase epitaxy (HVPE).

In our study, we didn't have a HVPE grown thick film. Instead, we rearranged our PL system as shown in Fig. 2-11. The laser used here was made by Kimmon, and was an originally vertical polarization beam. In such a case, the PL spectra of an UID-GaN were as shown Fig. 2-12. If we made the incident beam horizontal polarized, we could obtain some fraction of laser beam which has the electric field parallel to the c-axis [0001]. The spectra obtain is as shown in Fig. 2-13 which is similar to Reynolds's report [35]. However, the PL spectra measured at different temperatures were never been reported. As can be seem in Fig. 2-13, there are some split peaks near the band edge emission. As the temperature increased, the Γ_5 and Γ_6 was gradually merged. This phenomenon should

be explained by electron-spin coupling effect, as illustrated in Fig. 2-14 [23]. This is the valence bandedge structure around the VBM (valence band maximum) of WZ GaN. It shows the energy splitting at the top of the valence bands of GaN under the influence of crystal-field and spin-orbit coupling. The VBM is split into doubly degenerate Γ_6 and non-degenerate Γ_1 states even with the lack of the spin-orbit interaction. This energy splitting is called the crystal field splitting Δ_{cr}. Considering the spin-orbit interaction, the doubly degenerate Γ_6 state is split into Γ_9 and Γ_7 states, and the non-degenerate Γ_1 state is also labeled Γ_7. The energy splitting among these three states is called spin-orbit splitting Δ_{so}. At low temperatures, the electrons suffer less perturbation and are easily line-up and degenerated under polarized laser beam. As the temperature increases, the electrons were disturbed and hence no more degenerate Γ_9 and Γ_7 states.

2.4 2-DEG Phenomena of AlGaN/GaN Heterostructure Structures

The AlGaN/GaN heterostructure has been extensively examined due to its attractive 2DEG characteristics and has been widely employed in fabricating high-voltage and high-power electronic devices [24-26]. Unlike that of the $Al_xGa_{1-x}As$/GaAs heterostructure, for a given Al fraction, the piezoelectric effect at the AlGaN/GaN interface is very intense. As a result, the band discontinuity at the AlGaN/GaN interface is much more serious than at the $Al_xGa_{1-x}As$/GaAs interface [27]. J.P. Bergman published the first work on optical properties relating to the recombination of the 2DEG sub-band [28]. In recent years, several groups have presented the 2DEG photoluminescence (PL) spectra of the AlGaN/GaN heterostructures. A higher Al fraction (x=0.11~0.26) corresponds to superior 2DEG confinement [29]. Double confinement by incorporating a thin $Al_{0.12}Ga_{0.88}N$ in the

bottom side of the unintentionally doped (UID) GaN layer also improves 2DEG confinement [30]. Modifying the nucleation layer by inserting a thin AlN layer prior to i-GaN growth can improve both the mobility of 2DEG and crystal morphology [31]. The doping effect on the 2DEG PL spectra for the undoped and modulation-doped $Al_xGa_{1-x}N$/GaN heterostructures has also been reported [32]. In this section, we will describe the 2DEG phenomena of AlGaN/GaN hetero-structures. We will also elucidate the 2DEG sub-bands' photoluminescence spectra and their temperature dependence in details for various HEMT structures that were never clearly resolved before.

$Al_{0.15}Ga_{0.85}N$/GaN HEMTs were grown on a (0001) sapphire substrate using low-pressure metalorganic chemical vapor deposition (MOCVD) with an EMCORE D75 reactor. Hydrogen was employed as the carrier gas with silane, trimethylgallium, trimethylaluminum, and ammonia precursors. The HEMT structure consisted of Ohmic layer, Schottky layer, δ-doping electron donating layer , spacer, channel layer, nucleation layer and sapphire substrate. All the samples studied included a nucleation layer grown to around 400 Å at 500℃ and a 2 μm thick undoped GaN layer grown at 1040℃. Table III details each layer of the various samples used in this study. The Hall effect was measured using Bio-Rad 5900+ to determine the Hall mobility (μ_H) at room temperature (300 K) and at 77 K. The PL spectra at various temperatures were obtained by a 325 nm (3.815 eV) He-Cd laser excitation, the photon energy of which was sufficiently high to pump all the $Al_xGa_{1-x}N$ layers in the structures studied in this section.

The Hall measurements in Table III reveal that samples (a), (b) and (c) show high mobility at room temperature and at 77 K but sample (d) exhibits very low mobility. This result suggests that the enhanced 2DEG phenomena exist in the samples (a), (b) and (c) but not in (d). Figure 2-16 is a typical reflectivity spectrum

measured by EpiMetrics system. The growth rate of the u-GaN was easily measured in real-time. Each interface was also clearly identified. Figure 2-17 shows the PL spectra of all samples measured at 10 K. Note that some peaks are present below D^0X(3.486 eV) for all samples, but samples (a), (b) and (c) seem to show more peaks than does sample (d). We propose that these extra peaks are related to the 2DEG subbands emission. The sample (d) has a low Hall mobility (546 $cm^2/V \cdot s$) and does not exhibit 2DEG subbands' emission, perhaps due to the thin barrier layer causing a Coulombic interaction between the dopant and carriers. The sample (a) with a Hall mobility of 1221 $cm^2/V \cdot s$ and 5613 $cm^2/V \cdot s$ at 300 K and 77 K, respectively, exhibits weak 2DEG subbands' emission and strong $Al_{0.06}Ga_{0.94}N/Al_{0.20}Ga_{0.80}N$ PL emission (~3.60 eV), as shown in Fig. 2-17. The result is believed to be due to the absorption by the thick Ohmic layer and and Schottky layer. The sample (c) has a higher Al fraction in the electron Schottky layer, x=0.2, than does sample (b). A higher Al fraction corresponds to a smaller lattice constant. Thus, a stronger compression strain is induced across the 2DEG well, increasing the sheet concentration of the channel [33-34]. The increase in the Al fraction in the Schottky contact layer compresses the barrier; increases the bandgap of the spacer, and thus increases the ΔE_v across the interface of the 2DEG well.

The 2DEG is present at the interface of the AlGaN/GaN structure that is exactly at the interface of the spacer and the channel layer of a HEMT. Given that UID GaN is the thickest layer in these samples, so the PL spectra of UID GaN observed at a low temperature must be compared. The UID GaN has a Hall mobility of 131 ㎝$^2/V \cdot s$ with $N_s=2.41\times10^{13}$ ㎝$^{-2}$. Figure 2-13 shows the PL spectra of the UID GaN. The near band edge emission split into four subbands. The peak at 3.468 eV, corresponding to a neutral donor-bound exciton, referred to as D^0X, can be observed in the UID GaN and all the HEMTs structures in Fig. 2-17. The peaks in Fig. 2-18 differ greatly from that

in Fig. 2-13, this is due to the polarization effect of PL measurement in UID GaN [35]. As D. C. Reynolds *et. al.* reported, for $\mathbf{E} \perp c$ (making the electric field of a polarized laser beam normal to the *c*-axis) , D^0X dominates the near-band-edge emission of an UID GaN in the shape shown in Fig. 2-17. At the appropriate arrangement of sample orientation, making $\mathbf{E} \parallel c$, causes Γ_5 and Γ_6 to dominate the near-band-edge emission with a new A_L subband, implying that the grown UID GaN is of a very high quality material [25]. The 1'st phonon replica of the neutral donor bound exciton (D^0X-1LO) is present in the UID GaN and broadens as the temperature increases. In the contrast, for the sample (c) as shown in Fig. 2-18, the peaks close to 3.406 eV do not vary with the measured temperature of the HEMT. In particular, the peak at 3.406 eV does not appear in sample (b), as shown in Fig. 2-17. The shift of peak D^0X exceeds that of the 2DEG subbands when the PL-measuring temperature of sample (c) rises, since the triangular potential well varies little as the bands gap narrows. This result has been reported by other groups [31]. This discussion suggests that peaks below the D^0X correspond to transitions from 2DEG subbands to the valence band.

Figure 2-19 shows the energy separation (ΔE) of the 2DEG subbands from the GaN D^0X emission. Figure 2-18 clarifies the symbols. The two peaks nearest to D^0X, ΔE_m and ΔE_l, correspond to the observed 2DEG peaks in other reports [4-9]. B. Shen has demonstrated the temperature dependance of ΔE and found a downshift of around 3.5 meV from 10 K to 60 K. In the observed spectra, the shifts in ΔE_m and ΔE_l are approximately 4 meV and 1.2 meV respectively, which is consistent with Shen's report [30].

To verify whether the thinner spacer between the channel and the δ-doping layer really affected the 2-DEG mobility. It'd be better realized the carrier distributions, so we made the *C-V* measurements to calculate the depth profile. Comparing the sample c and sample d, they are almost the same structure, except for that the δ-doping layer

and the spacer were interchanged. The *C*-*V* measurement were performed at 1 MHz. The dielectric constants for each layer were estimated by the linear combination of the AlN and GaNs' according to the composition. The depth profiles may not be accurate enough due to the deviations from the calculated dielectric constant, but it really gave a qualitative explanation. The high concentration near the surface should be related to the n-GaN capping layer. The 2DEG should around at the depth of 540 Å from the surface. As expected, the sample d has broadened carrier distribution due to Coulombic interaction between the ionized dopants and electrons in the channel.

In summary, we have demonstrated the highly resolved PL spectra of 2DEG subbands in AlGaN/GaN HEMT structure that are consistent with the Hall measurement. There are at least five subbands observed in the HEMT structure in this study. The energy separation in the PL spectra between the interband transitions and near band edge transition are in the range of 25.1 meV to 172 meV. The strain has less effect on the subband transition than the near band edge transition that is consistent with other reports [34-35].

References in Chapter 2

[1] A.V. Davydov , W.J. Boettinger, U.R. Kattner, T.J. Anderson, "Thermodynamic Assessment of the Gallium-Nitrogen System", Phys. Stat. Sol. A, 2001, v. **188**, p. 407.

[2] H. Gotoh, S. Toru, H. Suzuki, and M. Kamata, Jpn. J. Appl. Phys. **20** (1981) L545.

[3] S. Yoshida, S. Gonda, and S. Misawa, J. Appl. Phys. **53** (1982) 6844.

[4] H. M. Manasevit, "Single-crystal gallium arsenide on insulating substrate", Appl. Phys. Lett., Vol. **12**, 156(1968).

[5] H. M. Manasevit, F. Erdmann and W. Simpson, J. Electrochem. Soc., Vol. 118, 1864(1971).

[6] I. P. Herman, "Optical diagnostics for Thin Film Processing", (Academic, Sand Diego, 1996).

[7] Frank L. Pedrotti, S. J. & Leno S. Pedrotti, Introduction to Optics, Second Edition. Upper Saddle River, New Jersey: Prentice-Hall, 1993.

[8] I. Akasaki, H. Amano, Y. Koide, K. Hiramatsu, N. Sawaki, Jounal of Crystal Growth 98, **209** (1989).

[9] S. Nakamura, Jpn. J. Appl. Phys. **30** (1991) 1620.

[10] J. N. Kuznia, M. Asif Khan, and D. T. Olson, J. Appl. Phys. **73** (1993) 4700.

[11] Landolt-Börnstein. Vol. 17. Springer. New York. (1982).

[12] .H. P. Maruska and J. J. Tietjen, Appl. Phys. Lett. 15,327 (1969).

[13] A. Estes Wickenden, D. K. Wickenden, and T, J. Kistenmacher, J. Appl. Phys. 75. 5367 (1994).

[14] J. N. Kuznia, M. Asif Khan, and D. T. Olson, J. Appl. Phys. 73. 4700 (1993)

[15] T. Sasaki, and T. Matsuoka, J. Appl. Phys. 77,192 (1995).

[16] B. Skromme, *Mater. Sci. Eng. B*, **50**, 117 (1998).

[17] J. J. Hopfield, J. Phys. Chem.. Solids, **15**, 97 (1960).

[18] D. W. Langer, R. N. Euwema, K. Era, T. Koda, Phys. Rev. B, **12**, 40005 (1970).

[19] C. F. Klingshirn, *Semiconductor Optics*, Springer-Verlag, Berlin, Heidelberg, New York, (1995)

[20] K. Cho, Phys. Rev. B., **14**, 4463 (1976).

[21] B. Gil, O. Briot, R. L. Aulombard, Phys. Rev. B, **52**, R17028 (1995).

[22] A. Hoffmann, L. Eckey, *Proc. Int. Conf. On Silicon Carbide and Related Wide Bandgap Materials Stockholm*, 1997.

[23] M. Suzuki and T. Uenoyama, "PROPERTIES, PROCESSING AND APPLICATION OF GALLIUM NITRIDE AND RELATED SEMICONDUCTOR", *EMIS Datareviews Series No. 23*, **A6.2**, 159 (1999).

[24] Y.-F. Wu, B.P. Keller, S. Keller, D. Kapolnek, P. Kozodoy, S.P. Denbaars, U.K. Mishra, Appl. Phys. Lett. **69,** 1438 (1996).

[25] R. Gaska, J.W. Yang, A. Osinsky, Q. Chen, M. Asif Khan, Appl. Phys. Lett **72,** 707 (1998).

[26] A. Qzgur, W. Kim, Z. Fan, A. Botchkarev, A. Salvador, S.N. Mohammad, B. Sverdlov, H. Morkoc, Electron. Lett. **31,** 1389 (1995).

[27] E.T. Yu, G.J. Sullivan, P.M. Asbeck, C.D. Wang, D. Qiao and S.S. Lau, Appl, Phys. Lett. **71,** 2794 (1997).

[28] J. P. Bergman, T. Lundström, B. Monemar, H. Amano and I. Akasaki, Appl. Phys. Lett. **69**, 3456-3458 (1996).

[29] G. Y. Zhao, H. Ishikawa, T. Egawa, T. Jimbo, M. Umeno, Physica E **7,** 963-966 (2000).

[30] B. Shen, T. Someya, O. Moriwaki, and Y. Arakawa, Appl. Phys. Lett. **76,** 679-681 (2000).

[31] L. K. Li, B. Turk, W. I. Wang, S. Syed, D. Simonian, and H. L. Stormer, Appl. Phys. Lett. **76**, 742-744 (2000).

[32] Ho Ki Kwon, C. J. Eiting, D. J. H. Lambert, B. S. Shelton, M. M. Wong, T.G. Zhu, and R. D. Dupuis, Journal of Crystal Growth **221**, 362-367 (2000).

[33] R. Gaska, J. W. Yang, A. D. Bykhovski, M. S. Shur, V. V. Kaminskii and S. Soloviov, Appl. Phys. Lett. **71**, 3817-3819 (1997).

[34] R. Gaska, J. W. Yang, A. D. Bykhovski, M. S. Shur, V. V. Kaminskii and S. Soloviov, Appl. Phys. Lett. **71**, 64-66 (1997).

[35] D. C. Reynolds, D. C. Look, B. Jogai, A. W. Saxler, S. S. Park and J. Y. Hahn, Appl. Phys. Lett. **77**, 2879-2881 (2000).